NANO LETTERS

Letter

pubs.acs.org/NanoLett

Long- versus Short-Range Scattering in Doped Epitaxial Graphene

C. Straßer,[†,▽] B. M. Ludbrook,[‡,§,▽] G. Levy,[‡,§] A. J. Macdonald,[‡,§] S. A. Burke,[‡,§,∥] T. O. Wehling,[⊥] K. Kern,[†,#] A. Damascelli,[‡,§] and C. R. Ast*[,†]

[†]Max Planck Institute for Solid State Research, 70569 Stuttgart, Germany

[‡]Department of Physics & Astronomy, University of British Columbia, Vancouver, British Columbia V6T 1Z1, Canada

[§]Quantum Matter Institute, University of British Columbia, Vancouver, British Columbia V6T 1Z4, Canada

[∥]Department of Chemistry, University of British Columbia, Vancouver, British Columbia V6T 1Z1, Canada

[⊥]Institut für Theoretische Physik, Universität Bremen, 28359 Bremen, Germany

[#]Institut de Physique de la Matière Condensée, Ecole Polytechnique Fédérale de Lausanne, 1015 Lausanne, Switzerland

ABSTRACT: Tuning the electronic properties of graphene by adatom deposition unavoidably introduces disorder into the system, which directly affects the single-particle excitations and electrodynamics. Using angle-resolved photoemission spectroscopy (ARPES) we trace the evolution of disorder in graphene by thallium adatom deposition and probe its effect on the electronic structure. We show that the signatures of quasiparticle scattering in the photoemission spectral function can be used to identify thallium adatoms, although charged, as efficient short-range scattering centers. Employing a self-energy model for short-range scattering, we are able to extract a δ-like scattering potential $\delta = -3.2 \pm 1$ eV. Therefore, isolated charged scattering centers do not necessarily act just as good long-range (Coulomb) scatterers but can also act as efficient short-range (δ-like) scatterers; in the case of thallium, this happens with almost equal contributions from both mechanisms.

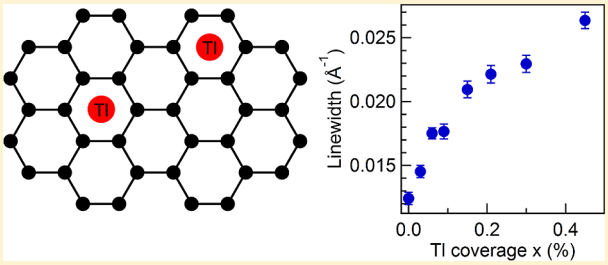

KEYWORDS: *Graphene, long-range (Coulomb) scattering, short-range scattering, self-energy, angular resolved photoemission spectroscopy*

Many interesting properties of graphene can be tuned by the appropriate introduction of impurities. This concerns not just charge-transfer doping through adatoms or molecules to tune the position of the Dirac point with respect to the Fermi level[1−5] but also different interactions (electron−electron or electron−phonon),[6−8] metal−insulator transitions,[9,10] and, so far only at the level of theoretical prediction, the emergence of superconductivity[11] or of topologically insulating behavior.[12] However, those same impurities give rise to unavoidable mobility-limiting disorder and enhanced scattering.[14] Efficient doping by molecules even necessitates the presence of defects in the graphene layer.[15] In most cases, adatoms reduce the quasiparticle lifetime by introducing long-range (Coulomb) scattering and/or short-range (δ-potential) scattering, which has been proposed to be largely responsible for graphene's residual conductivity.[14]

The way an impurity modifies the electronic structure depends on how it interacts with the graphene layer, i.e., donating charge to the graphene layer and acting as a charged impurity, or being attached in some way to the graphene layer. This ranges from weakly attached physisorption[16] to the formation of a covalent bond as in the example of hydrogen, which sp^3-hybridizes the carbon bond severely affecting the graphene electronic structure.[9] While it is generally agreed upon that the charge carrier mobility μ is inversely proportional to the density of charged impurities n_{imp}, resulting in an increase of the scattering rate upon doping, other reports claim an increase of the quasiparticle lifetime upon doping with charged impurities.[17] Such behavior critically depends on screening, which is determined through the dielectric constant ϵ of the system.

Although Coulomb scattering is often assumed to be the dominant scattering mechanism in graphene, short-range scattering can become appreciable if dielectric screening is highly effective in reducing Coulomb scattering relative to short-range scattering or if there are impurity states (of the unperturbed impurity) close to the Fermi level giving rise to a particularly strong scattering potential. In this sense, short-range scattering can also be present for noncovalently bonded impurities. Therefore, in real systems, it is not necessarily a priori clear which scattering mechanism is dominant.

Here, we use the experimental spectral function measured by angle-resolved photoemission spectroscopy (ARPES) on thallium-doped epitaxial graphene to observe the scattering behavior induced by the thallium adatoms and disentangle Coulomb (long-range) from δ-like (short-range) scattering contributions. Thallium on graphene is a particularly interesting

Received: October 29, 2014
Revised: March 25, 2015
Published: March 30, 2015

DOI: 10.1021/nl504155f
Nano Lett. 2015, 15, 2825−2829

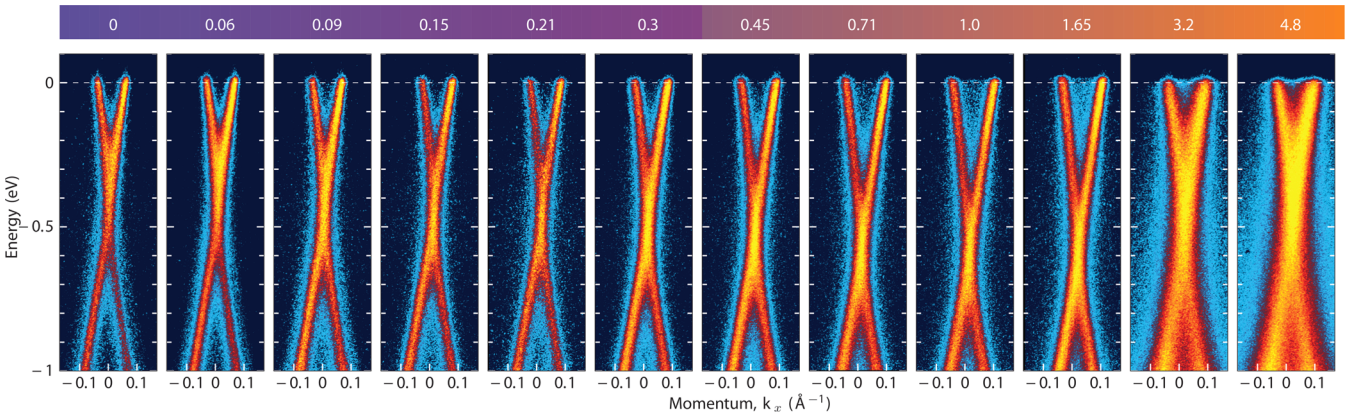

Figure 1. Monolayer graphene decorated with small amounts of thallium atoms. Experimental band structure near the $\bar{K}$-point for increasing Tl concentration x (given in % in the upper bar) measured at 8 K with a photon energy of 40.8 eV.

model system as it nicely demonstrates the difficulty to predict the scattering behavior beforehand. We show that it features a sizable short-range scattering contribution although its adsorption behavior is similar to potassium: it is extremely weakly bonded to graphene and highly mobile at temperatures above 15 K. Only by employing the electronic structure of the unperturbed thallium atom, we are able to theoretically predict the scattering behavior. In addition, thallium has been proposed as one of the most promising candidates to open a spin−orbit coupling related gap at the Dirac point turning graphene into a topological insulator.[12] Exploiting the fact that correlation effects are suppressed at the Fermi level (Luttinger's theorem), at low temperature the spectral line width at the Fermi level reflects predominantly defect and disorder contributions. Both long-range and short-range scattering mechanisms can be described by an analytic expression for the self-energy in the dilute limit. Fitting the self-energy to the experimental data allows us to extract the fundamental parameters of the scattering mechanisms at play in the graphene layers.

Figure 1 shows the experimental band structure of an epitaxial graphene monolayer near the $\bar{K}$-point as a function of thallium deposition.[13] The concentration x of thallium atoms on the surface is given in percent of a graphene monolayer, i.e., the number of thallium atoms per carbon atom. The left-hand side data set is from the pristine graphene monolayer, exhibiting an initial n-type doping due to the intrinsic charge transfer from the SiC substrate. Upon thallium deposition, electron doping increases so that the Dirac point shifts to higher binding energies, away from the Fermi level. We attribute this to charge transfer from the thallium atoms to the graphene. For concentrations higher than 1%, the trend is reversed, and the Dirac point shifts back toward the Fermi level. We ascribe this to the statistical effect that, for concentrations higher than about 1%, pairing and clustering of atoms become non-negligible, which reduces the efficiency of charge transfer doping. For this reason in the following we will concentrate on the dilute limit below 1%, where clustering effects can be neglected.

Scanning tunneling microscopy (STM) measurements demonstrate that at very low temperatures and concentrations thallium atoms are present as immobile monomers on the surface (see Figure 2a). The topographic image shows a thallium covered graphene monolayer for a coverage of 0.2%. Even at this low coverage, a small fraction of adsorbed thallium appears to be in dimer or trimer form, although the vast majority appears to be thallium monomers. This has also been confirmed by Tl deposition on a clean Au(111) surface using the same parameters and yielding the same number density. Although the large apparent size of the thallium adatoms and graphene's inherent electronic inhomogeneity make an identification of the adsorption site difficult, thallium on more uniform graphene patches appears to sit on the hollow site, in agreement with density functional theory (DFT) calculations.[12] As the precise coverage is important for the subsequent quantitative analysis of the ARPES data, the STM results were also used for the precise flux calibration of the thallium evaporator.

While the thallium atoms were immobile below 8 K in the topographic image (Figure 2a), we observe that thallium atoms are extremely mobile on the graphene surface at higher temperatures (cf. refs 13 and 18). This is illustrated in the temperature dependence of the relative energy shift of the Dirac point in Figure 2b for a Tl coverage of 0.5%. Above 15 K, a rapid decrease in doping efficiency can be observed, which we attribute to clustering of Tl atoms. We conclude that Tl is only very weakly and not covalently bonded to the graphene similar to alkali atoms.

The shift of the Dirac point to higher binding energies upon thallium deposition illustrated in Figure 1 corresponds to an increase of the Fermi surface volume. The corresponding evolution of Fermi wave vector k_F as well as charge carrier density n and energy shift are shown in Figure 2c,d, respectively. Below a coverage of 1%, all three parameters are increasing monotonically. The energy shift reflects the increase in occupation due to the donation of electrons by the thallium atoms. A simple model employing graphene's linear density of states is used to estimate the number of electrons donated per thallium atom. The best fit is found for 1.0 electrons donated by a thallium atom to the graphene layer. This is also in excellent agreement with recent DFT calculations for thallium adatoms on graphene.[12]

At a constant low temperature, line width broadening at the Fermi level from interactions (i.e., electron−electron, electron−phonon, and electron−plasmon) can be regarded as a small, constant contribution. In a Fermi liquid, line width broadening at the Fermi level due to interactions vanishes as T^2 when the temperature goes to zero. Consequently, constant contributions are predominantly due to scattering from disorder such as impurities and defects. The line widths carrying the scattering information are taken from the full-width at half-maximum

DOI: 10.1021/nl504155f
Nano Lett. 2015, 15, 2825−2829

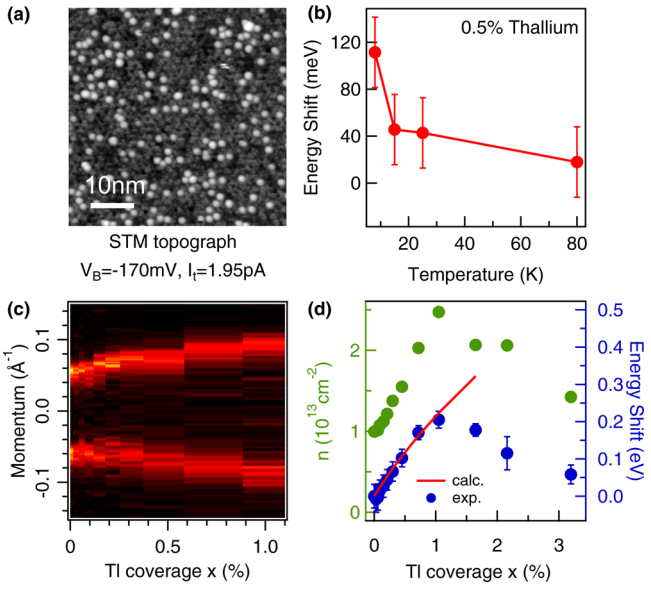

Figure 2. Coverage and temperature dependency. (a) STM topograph of a Tl covered graphene surface (x = 0.2%) at a temperature of 4.5 K. The Tl atoms appear as large protrusions with diameter of about 2 nm. (b) Temperature dependence of the doping efficiency. The energy axis shows the energy shift of the Dirac point relative to the clean graphene sample. (c) Evolution of the Fermi wave vector k_F about $\bar{K}$ for increasing Tl coverage x. (d) Charge carrier density as well as experimental and calculated energy shift of the Dirac point as a function of Tl coverage x.

(fwhm) of momentum distribution curves (MDCs) at the Fermi level; these are shown as a function of thallium coverage in Figure 3. They were extracted by fitting the MDCs with a Voigt function, a convolution of a Gaussian and Lorentzian, as illustrated in Figure 3a; the width of the Gaussian resolution function was set to match the experimental momentum resolution 0.016 Å^{-1}, while the line width, presented in Figure 3b, corresponds to the fwhm of the Lorentzian line shape.

Upon increasing the thallium coverage in Figure 3, the line width increases monotonically. This is due to scattering from the randomly adsorbed thallium atoms, which will be the focus of the reminder of this study. We assume that the line width we measure for the clean sample comes from initial disorder, defects, and residual interactions and enters as a constant offset in every measurement. This assumption is justified as long as we stay at a constant low temperature, which results in small contributions from interactions. We exclude contributions to the line width from plasmarons because of the presence of defect scattering in the pristine graphene, which easily suppresses their spectral weight.[19−21] In order to unravel the contributions from the thallium-induced disorder to the line width broadening and thus the corresponding contribution to graphene's electrodynamics, we discuss two scattering mechanisms in more detail.

The first mechanism is due to scattering from charged impurities, which has a long-range effect due to the screened Coulomb potential. Since thallium donates one electron per atom to the graphene sheet, it can be treated as a long-range Coulomb scatterer. The line width broadening, which can be directly modeled by the imaginary part of the self-energy, has the following simplified expression:

$$\mathrm{Im}\,\Sigma_{\mathrm{long}} = \alpha^2 n_{\mathrm{imp}} v_F \pi I(2\alpha)/k_F \qquad (1)$$

where α is the effective fine-structure constant, $I(2\alpha)$ is a function defined in ref 22, v_F is the Fermi velocity, n_{imp} is the impurity density (which relates to the thallium concentration x via $n_{\mathrm{imp}} = 2x/A$, where A is the area of the graphene unit cell), and $k_F = (\pi(\eta n_{\mathrm{imp}} + \eta_0))^{1/2}$ is the Fermi momentum with η being the number of electrons donated per impurity atom and η_0 the charge density in graphene before thallium deposition.

The only free parameter in eq 1 is the effective fine-structure constant of graphene; all other parameters can be determined from the experiment. The effective fine structure constant depends on the dielectric constant ϵ through $\alpha = 2.2/\epsilon$. The dielectric constant in turn is determined by the underlying substrate; the smaller its value, the stronger the long-range scattering contribution to the line width broadening. From the analysis of plasmaron signatures in epitaxial graphene on a buffer layer on SiC(0001),[23] the dielectric constant has been determined to be $\epsilon = 22 \pm 8$. The long-range scattering calculated from eq 1 using this value of ϵ is shown in Figure 3b in red and clearly does not fit the measured line width evolution with thallium coverage. Because of the charge carrier screening supported by the substrate, the value of ϵ for epitaxial graphene is expected to be larger than for freestanding graphene. Recent calculations, however, point toward an overestimate of the dielectric constant,[24] suggesting that the actual value is likely smaller. Indeed, by analyzing the band velocity renormalization in epitaxial graphene, a reduced value $\epsilon = 7.26 \pm 0.02$ was found.[25] The line width broadening from long-range scattering for this value of the dielectric constant is shown as a yellow line in Figure 3b. It also just accounts for part of the experimental line width broadening. Therefore, another mechanism is likely to contribute to the experimental line width.

A second prominent scattering mechanism that arises in the presence of disorder is short-range scattering from an effective δ-potential. This approach does not distinguish between inter- and intravalley scattering in graphene, but it gives a general trend about the strength of short-range scattering. The long-range Coulomb potential and the short-range potential affect the Dirac electrons very differently. The Coulomb potentials associated with the Tl adatoms (charge +1) are subcritical.[35] Consequently, there are no quasi bound states associated with the Coulomb scattering alone. However, the short-range scatterers cause characteristic resonances as manifesting for

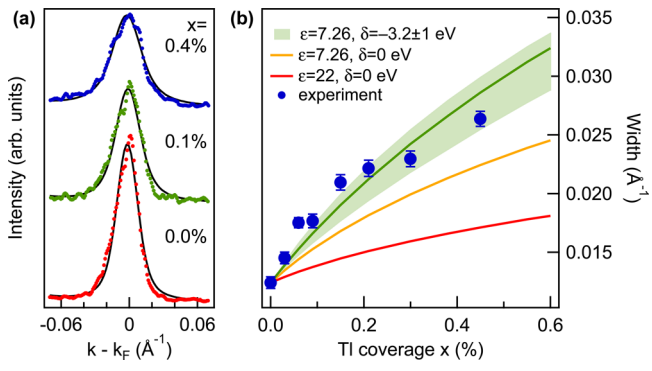

Figure 3. Analysis of the experimental line width at the Fermi level. (a) Momentum distribution curves (MDCs) at the Fermi level for different Tl coverages x with the corresponding fitted Voigt functions. (b) Increase of the line width as a function of Tl coverage x and the results of the model calculations using different parameters. Because of the strongly nonlinear behavior of the function, the shaded green region is not symmetric around the green line.

DOI: 10.1021/nl504155f
Nano Lett. 2015, 15, 2825−2829

instance in the self-energy shown in Figure 4. These resonances are associated with quasi localized impurity states, which exhibit enhanced density of states in the vicinity of the impurity at certain resonant energies (cf. ref 27).

Short-range scattering is appreciable when adatoms have states close to the Fermi level, thereby inducing a sizable scattering potential.[26,27] Its effect on the line width broadening can be modeled by the self-energy within the Wolff−Clogston model.[28,29] We adopt a self-consistent implementation in the dilute limit within the coherent potential approximation:[30]

$$\mathrm{Im}\,\Sigma_{\mathrm{short}}(\omega) = x\delta\,\mathrm{Im}\left(1 + \frac{\delta G^0(\omega - \Sigma(\omega))}{1 - \delta G^0(\omega - \Sigma(\omega))}\right) \quad (2)$$

where $G^0(\omega)$ is the lattice Green's function of the unperturbed graphene lattice[31] and δ is the scattering potential. As the thallium concentration x as well as the lattice Green's function are known, the only free parameter in the short-range scattering model is the scattering potential parameter δ.

To evaluate the combined effect of both scattering processes, we add the self-energies for long-range and short-range scattering and calculate the theoretical line width.[32] To this end, we note that ϵ and δ cannot be found simultaneously based on our scattering analysis; however, using the experimentally determined value of ϵ from ref 22, δ remains as the only unknown parameter and can thus be determined directly from the observed line width evolution versus thallium concentration. We find good agreement with the experimental data for $\epsilon = 7.26$ and $\delta = -3.2 \pm 1$ eV (see shaded green area in Figure 3b). As it turns out, the contributions from short-range and long-range scattering have comparable magnitudes.

The overall behavior of the imaginary part of the short-range scattering self-energy for graphene is shown in Figure 4. Its rather strong energy dependence is due to the special energy dependence of the graphene lattice Green's function in conjunction with that of the scattering potential itself. The dependence on the scattering potential δ at an energy $\omega = 0.5$ eV, thus in the vicinity of the experimentally relevant energies, is shown in the inset of Figure 4. For $\delta \to \pm\infty$, which can be interpreted as a missing atom in the lattice, the imaginary part approaches the same finite value. For small values of δ, we see that the imaginary part of the self-energy varies more rapidly, although it remains bounded. Therefore, the contribution from short-range scattering to line width broadening is limited for $\omega \gtrsim 0.5$ eV, but not necessarily negligible, and exhibits a maximum value for $\delta \approx -5$ eV.

When comparing the value here obtained for δ with available calculations in the literature,[12] we have to keep in mind that our short-range scattering model does not distinguish between different angular momentum channels, but rather attributes equal scattering amplitude to all scattering channels. It may be the simplest model with only one free parameter, but it still gives a measure for the strength of the short-range scattering. We can obtain a ballpark estimate for δ from the formula $\delta = t_{\mathrm{ad}}^2/|\Delta E|$, where t_{ad} is the hopping to the Tl adatom and ΔE is the energy difference between the unperturbed (free) Tl adatom states and the Fermi level.[26,27] From the parameters reported in ref 12, we can estimate a theoretical δ_{th} value ranging between −1 to −4 eV. Therefore, our results suggest that short-range scattering in this system lies on the larger side of the theoretically predicted range.

Similar effects of enhanced scattering due to impurities have been observed in a number of transport experiments,[14,33,34] in agreement with our findings. There, the main scattering indicator is the carrier mobility, which decreases linearly with increasing impurity density. By contrast, a decreasing photoemission line width upon potassium doping has been reported by Siegel et al.[7] We attribute this variance to the different doping regime and correspondingly different intrinsic screening that were probed in the experiments. Carrier scattering mechanisms in graphene (including charge impurities, resonant scatterers, and ripples) have been strongly debated,[14,35] and predominance of one or the other mechanism is largely sample dependent. For graphene subjected to charged impurities, e.g., alkali adatoms, long-range scattering is typically expected to be much more effective in charge carrier scattering than short-range scattering.[33,36,37] Thallium adatoms on graphene, having an impurity charge of +1, might be expected to behave in a similar fashion. We showed, however, that this is a system where both mechanisms have nearly equal contributions due to the proximity of thallium impurity states to the Fermi level. More generally, this implies that it cannot be a priori assumed what scattering mechanism will dominate in any given impurity−graphene system.

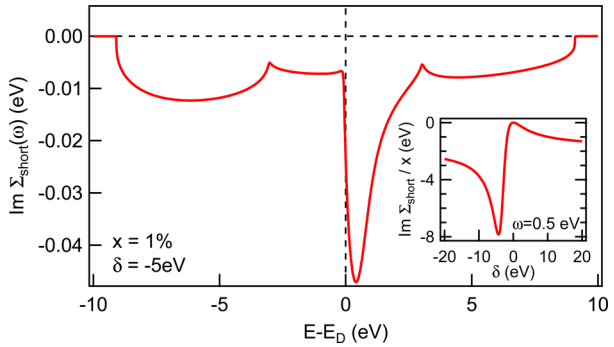

Figure 4. Short-range scattering model. Imaginary part of the self-energy for the short-range scattering. Inset: self-energy as a function of scattering potential δ at constant energy and normalized with respect to the Tl coverage.

In summary, we have quantitatively shown that Tl adatoms on a monolayer of epitaxial graphene grown on a buffer layer on SiC(0001) not only show electron doping but also have a large effect on the quasiparticle scattering rate. Concerning the enhanced spin−orbit gap predicted for Tl on graphene,[12] we found that a possible gap opening is likely masked by the disorder broadening, which will make it unlikely to observe such a small gap in photoemission directly. Also, recent transport studies of indium on graphene did not show any enhanced spin−orbit signature.[38] To suppress the line width broadening due to disorder, one would have to, e.g., arrange the Tl atoms in a regular lattice on the graphene monolayer. In the present study, however, the Tl adatoms introduce disorder and act on the graphene electronic structure both as Coulomb long-range scatterers and short-range scatterers with a δ-like potential. By modeling the self-energy for both scattering mechanisms, we are able to extract a strong short-range scattering potential $\delta = -3.2 \pm 1$ eV. The short-range scattering contribution can be strong for both covalent and ionically bound impurities, if the impurity provides a resonance sufficiently close to the Fermi level. Thus, short-range scattering can contribute to a sizable increase of the scattering rate, even in the case of charged impurities where long-range Coulomb scattering is usually expected to dominate. These findings and the ability to predict and/or account for conflating scattering

DOI: 10.1021/nl504155f
Nano Lett. 2015, 15, 2825−2829

mechanisms will have important implications in the development of novel impurity−graphene-based electronics.

AUTHOR INFORMATION

Corresponding Author

*E-mail: c.ast@fkf.mpg.de.

Author Contributions

[▽]These authors contributed equally to the work.

Notes

The authors declare no competing financial interest.

ACKNOWLEDGMENTS

The authors thank U. Starke and S. Forti from MPI-FKF in Stuttgart for hydrogen etching of the SiC substrates and growing of the monolayer graphene samples in argon gas. We gratefully acknowledge M. Franz, J. A. Folk, G. A. Sawatzky, and M. W. Haverkort for discussions. C.R.A. acknowledges funding from the Emmy-Noether-Program of the Deutsche Forschungsgemeinschaft (DFG). The work at UBC was supported by the Max Planck-UBC Centre for Quantum Materials, the Killam, Alfred P. Sloan, Alexander von Humboldt, and NSERC's Steacie Memorial Fellowships (to A.D.), the Canada Research Chairs Program (to A.D. and S.A.B.), NSERC, CFI, and CIFAR Quantum Materials.

REFERENCES

(1) Chen, W.; Chen, S.; Qi, D. C.; Gao, X. Y.; Wee, A. T. S. *J. Am. Chem. Soc.* **2007**, *129*, 10418.

(2) Coletti, C.; Riedl, C.; Lee, D. S.; Krauss, B.; Patthey, L.; von Klitzing, K.; Smet, J. H.; Starke, U. *Phys. Rev. B* **2010**, *81*, 235401.

(3) Gierz, I.; Riedl, C.; Starke, U.; Ast, C. R.; Kern, K. *Nano Lett.* **2008**, *8*, 4603.

(4) Pi, K.; McCreary, K. M.; Bao, W.; Han, W.; Chiang, Y. F.; Li, Y.; Tsai, S.-W.; Lau, C. N.; Kawakami, R. K. *Phys. Rev. B* **2009**, *80*, 075406.

(5) Wehling, T. O.; Novoselov, K. S.; Morozov, S. V.; Vdovin, E. E.; Katsnelson, M. I.; Geim, A. K.; Lichtenstein, A. I. *Nano Lett.* **2008**, *8*, 173.

(6) Bostwick, A.; Ohta, T.; Seyller, T.; Horn, K.; Rotenberg, E. *Nat. Phys.* **2007**, *3*, 36.

(7) Siegel, D. A.; Park, C.-H.; Hwang, C.; Deslippe, J.; Fedorov, A. V.; Louie, S. G.; Lanzara, A. *Proc. Natl. Acad. Sci.* **2011**, *108*, 11365.

(8) McChesney, J. L.; Bostwick, A.; Ohta, T.; Seyller, T.; Horn, K.; González, J.; Rotenberg, E. *Phys. Rev. Lett.* **2010**, *104*, 136803.

(9) Bostwick, A.; McChesney, J. L.; Emtsev, K. V.; Seyller, T.; Horn, K.; Kevan, S. D.; Rotenberg, E. *Phys. Rev. Lett.* **2009**, *103*, 056404.

(10) Schubert, G.; Fehske, H. *Phys. Rev. Lett.* **2012**, *108*, 066402.

(11) Profeta, G.; Calandra, M.; Mauri, F. *Nat. Phys.* **2012**, *8*, 131.

(12) Weeks, C.; Hu, J.; Alicea, J.; Franz, M.; Wu, R. *Phys. Rev. X* **2011**, *1*, 021001.

(13) Epitaxial graphene monolayers with a buffer layer were grown under Ar atmosphere on hydrogen annealed 6H-SiC(0001) in Stuttgart. ARPES and STM measurements were performed in Vancouver. For ARPES, we used a SPECS Phoibos 150 hemispherical analyzer with linearly polarized 40.8 eV photons from a UVS300 monochromatized gas discharge lamp. The resolution was set to 15 meV and 0.3°. As thallium is one of the most mobile atoms on the graphene surface,[18] we evaporated from an e-beam evaporator on a cold sample to avoid surface diffusion (at 4.5 K for STM and 8 K for ARPES). All measurements were also done in the same temperature range. The pressure during measurements was better than 7×10^{-11} mbar.

(14) Peres, N. M. R. *Rev. Mod. Phys.* **2010**, *82*, 2673.

(15) Medina, H.; Lin, Y.-C.; Obergfell, D.; Chiu, P.-W. *Adv. Funct. Mater.* **2011**, *21*, 2687.

(16) Schedin, F.; Geim, A. K.; Morozov, S. V.; Hill, E. W.; Blake, P.; Katsnelson, M. I.; Novoselov, K. S. *Nat. Mater.* **2007**, *6*, 652.

(17) Siegel, D. A.; Regan, W.; Fedorov, A. V.; Zettl, A.; Lanzara, A. *Phys. Rev. Lett.* **2013**, *110*, 146802.

(18) Nakada, K.; Ishii, A. *Solid State Commun.* **2011**, *151*, 13.

(19) Hwang, E. H.; Das Sarma, S. *Phys. Rev. B* **2008**, *77*, 081412.

(20) Polini, M.; Asgari, R.; Borghi, G.; Barlas, Y.; Pereg-Barnea, T.; MacDonald, A. H. *Phys. Rev. B* **2008**, *77*, 081411.

(21) Bostwick, A.; Speck, F.; Seyller, T.; Horn, K.; Polini, M.; Asgari, R.; MacDonald, A. H.; Rotenberg, E. *Science* **2010**, *328*, 999.

(22) Hwang, E. H.; Das Sarma, S. *Phys. Rev. B* **2008**, *77*, 195412.

(23) Walter, A. L.; et al. *Phys. Rev. B* **2011**, *84*, 085410.

(24) Lischner, J.; Vigil-Fowler, D.; Louie, S. G. *Phys. Rev. Lett.* **2013**, *110*, 146801.

(25) Hwang, C.; Siegel, D. A.; Mo, S.-K.; Regan, W.; Ismach, A.; Zhang, Y.; Zettl, A.; Lanzara, A. *Sci. Rep.* **2012**, *2*, 590.

(26) Robinson, J. P.; Schomerus, H.; Oroszlány, L.; Fal'ko, V. I. *Phys. Rev. Lett.* **2008**, *101*, 196803.

(27) Wehling, T. O.; Katsnelson, M. I.; Lichtenstein, A. I. *Chem. Phys. Lett.* **2009**, *476*, 125.

(28) Clogston, A. M.; Matthias, B. T.; Peter, M.; Williams, H. J.; Corenzwit, E.; Sherwood, R. C. *Phys. Rev.* **1962**, *125*, 541.

(29) Wolff, P. A. *Phys. Rev.* **1961**, *124*, 1030.

(30) Velický, B.; Kirkpatrick, S.; Ehrenreich, H. *Phys. Rev.* **1968**, *175*, 747.

(31) Horiguchi, T. *J. Math. Phys.* **1972**, *13*, 1411.

(32) The theoretical line widths have been determined by an analogous Lorentzian MDC fit procedure performed at the appropriate binding energy, corresponding to the position of the Fermi level in the experiment, on a theoretical spectral function calculated from graphene's single particle Green's function with the inclusion of self-energies (eqs 1 and/or 2) and a constant residual broadening.

(33) Tan, Y.-W.; Zhang, Y.; Bolotin, K.; Zhao, Y.; Adam, S.; Hwang, E. H.; Das Sarma, S.; Stormer, H. L.; Kim, P. *Phys. Rev. Lett.* **2007**, *99*, 246803.

(34) Das Sarma, S.; Adam, S.; Hwang, E. H.; Rossi, E. *Rev. Mod. Phys.* **2011**, *83*, 407.

(35) Katsnelson, M. I. *Graphene: Carbon in Two Dimensions*; Cambridge University Press: Cambridge, U.K., 2012.

(36) Hwang, E.; Adam, S.; Das Sarma, S. *Phys. Rev. Lett.* **2007**, *98*, 186806.

(37) Nomura, K.; MacDonald, A. H. *Phys. Rev. Lett.* **2007**, *98*, 076602.

(38) Jia, Z.; Yan, B.; Niu, J.; Han, Q.; Zhu, R.; Wu, X.; Yu, D. arXiv: 1409.8090; 2014.

DOI: 10.1021/nl504155f
Nano Lett. 2015, 15, 2825−2829